Strong mean field dynamos require supercritical helicity fluxes

A. Brandenburg[1] and K. Subramanian[2]

[1] NORDITA, Blegdamsvej 17, 2100 Copenhagen Ø, Denmark
[2] IUCAA, Post Bag 4, Pune University Campus, Ganeshkhind, Pune 411 007, India

Abstract. Several one and two dimensional mean field models are analyzed where the effects of current helicity fluxes and boundaries are included within the framework of the dynamical quenching model. In contrast to the case with periodic boundary conditions, the final saturation energy of the mean field decreases inversely proportional to the magnetic Reynolds number. If a nondimensional scaling factor in the current helicity flux exceeds a certain critical value, the dynamo can operate even without kinetic helicity, i.e. it is based only on shear and current helicity fluxes, as first suggested by Vishniac & Cho (2001, ApJ 550, 752). Only above this threshold is the current helicity flux also able to alleviate catastrophic quenching. The fact that certain turbulence simulations have now shown apparently non-resistively limited mean field saturation amplitudes may be suggestive of the current helicity flux having exceeded this critical value. Even below this critical value the field still reaches appreciable strength at the end of the kinematic phase, which is in qualitative agreement with dynamos in periodic domains. However, for large magnetic Reynolds numbers the field undergoes subsequent variations on a resistive time scale when, for long periods, the field can be extremely weak.

Key words: MHD – turbulence

1. Introduction

Astrophysically relevant dynamos tend to have boundaries or are at least confined. In all practically relevant cases they are certainly not homogeneous. Exceptions are dynamos on the computer where triply-periodic boundary conditions are used. Despite such dynamos being so unrealistic, they have played an enormously important role in revealing the nature of catastrophic α quenching (Brandenburg 2001, hereafter referred to as B01; Blackman & Brandenburg 2002, hereafter referred to as BB02). This applies in particular to the case of helically forced turbulence. For reviews regarding recent developments see Brandenburg et al. (2002) and Brandenburg & Subramanian (2005a). However, some important conclusions drawn from triply periodic simulations do not carry over to the case with boundaries. In this paper we discuss in particular the saturation field strength and focus on the mean-field description taking the evolution equation of current helicity with the corresponding current helicity fluxes into account.

Homogeneous turbulent dynamos saturate in such a way that the total current helicity vanishes, i.e. $\langle \boldsymbol{J} \cdot \boldsymbol{B} \rangle = 0$, where

Correspondence to: brandenb@nordita.dk

$\boldsymbol{B}$ is the magnetic field, $\boldsymbol{J} = \boldsymbol{\nabla} \times \boldsymbol{B}/\mu_0$ the current density, and μ_0 is the vacuum permeability. (Here and below, $\langle ... \rangle$ denotes volume averages.) This is a direct result of magnetic helicity conservation in the absence of boundaries (B01). If the turbulence is driven at a scale smaller than the box size L, i.e. the forcing wavenumber k_f exceeds the box wavenumber $k_1 = 2\pi/L$ (so $k_\mathrm{f} \gg k_1$), it makes sense to use a two-scale approach. We therefore write $\boldsymbol{B} = \overline{\boldsymbol{B}} + \boldsymbol{b}$ and $\boldsymbol{J} = \overline{\boldsymbol{J}} + \boldsymbol{j}$, where the overbar denotes an average field suitably defined over one or sometimes two periodic coordinate directions, and lower case characters denote the fluctuations. The condition of zero current helicity then translates to

$$\langle \overline{\boldsymbol{J}} \cdot \overline{\boldsymbol{B}} \rangle = -\langle \boldsymbol{j} \cdot \boldsymbol{b} \rangle \quad \text{(no boundaries).} \tag{1}$$

Together with the assumption that the large and small scale fields are nearly fully helical and that the sign of the helicity of the forcing is positive, we have $\langle \overline{\boldsymbol{J}} \cdot \overline{\boldsymbol{B}} \rangle \approx -k_1 \langle \overline{\boldsymbol{B}}^2 \rangle/\mu_0$ and $\langle \boldsymbol{j} \cdot \boldsymbol{b} \rangle \approx k_\mathrm{f} \langle \boldsymbol{b}^2 \rangle/\mu_0$. The important conclusion from this is that, in the steady state, the amplitude of the mean field exceeds that of the small scale field, with

$$\langle \overline{\boldsymbol{B}}^2 \rangle \approx \frac{k_\mathrm{f}}{k_1} \langle \boldsymbol{b}^2 \rangle \quad \text{(no boundaries).} \tag{2}$$

Moreover, for large enough magnetic Reynolds numbers the small scale magnetic energy is in rough equipartition with the

turbulent kinetic energy, i.e. $\langle \boldsymbol{b}^2 \rangle / \mu_0 \approx \langle \rho \boldsymbol{u}^2 \rangle$, but see BB02 for a more accurate estimate for intermediate values of the magnetic Reynolds number. In the case considered in B01, where the scale separation ratio k_{f}/k_1 is either 5 or 30, the mean field amplitude exceeds the equipartition value by about 5 or 30 – independent of the magnetic Reynolds number.

The assumption of full homogeneity, which can only be realized with triply periodic boundary conditions, was an important ingredient in arriving at super-equipartition fields. In this paper we discuss the more general case of non-periodic boundary conditions. We use here a mean-field approach together with the dynamical quenching model (Kleeorin & Ruzmaikin 1982; Kleeorin et al. 1995), which proved successful in reproducing the homogeneous case as it was obtained using direct simulations (Field & Blackman 2002; BB02; Subramanian 2002). In the steady state without helicity fluxes, the dynamical quenching model agrees with a modified catastrophic quenching formula which includes a term from the current helicity of the large scale field (Gruzinov & Diamond 1994, 1995; BB02).

2. Description of the model

In the mean field approach we solve the induction equation for the mean magnetic field $\overline{\boldsymbol{B}}$ together with an evolution equation for the magnetic component of the α effect,

$$\frac{\partial \overline{\boldsymbol{B}}}{\partial t} = \boldsymbol{\nabla} \times (\overline{\boldsymbol{U}} \times \overline{\boldsymbol{B}} + \overline{\boldsymbol{\mathcal{E}}} - \eta \overline{\boldsymbol{J}}), \tag{3}$$

$$\frac{\partial \alpha_{\mathrm{M}}}{\partial t} = -2\eta_{\mathrm{t}} k_{\mathrm{f}}^2 \left(\frac{\overline{\boldsymbol{\mathcal{E}}} \cdot \overline{\boldsymbol{B}} + \frac{1}{2} k_{\mathrm{f}}^{-2} \boldsymbol{\nabla} \cdot \overline{\boldsymbol{\mathcal{F}}}_C^{\mathrm{SS}}}{B_{\mathrm{eq}}^2} + \frac{\alpha_{\mathrm{M}}}{R_{\mathrm{m}}} \right), \tag{4}$$

where current density is measured in units where $\mu_0 = 1$, η is the microscopic magnetic diffusivity, η_{t} is the turbulent magnetic diffusivity, $R_{\mathrm{m}} = \eta_{\mathrm{t}}/\eta$ is the magnetic Reynolds number, $\overline{\boldsymbol{\mathcal{E}}}$ is the mean electromotive force that includes, among other terms, a term proportional to $\alpha_{\mathrm{M}}\overline{\boldsymbol{B}}$. In the following we adopt the numerical value $k_{\mathrm{f}}/k_1 = 5$ for the scale separation ratio. The derivation of the α_{M} equation is this normalization can be found in BB02 without helicity flux and in Brandenburg & Sandin (2004, hereafter BS04) with helicity flux. The connection with $\alpha_{\mathrm{M}} = \frac{1}{3}\tau \overline{\boldsymbol{j} \cdot \boldsymbol{b}}$ has been accomplished by using the definitions $B_{\mathrm{eq}}^2 = \mu_0 \rho u_{\mathrm{rms}}^2$ and $\eta_{\mathrm{t}} = \frac{1}{3}\tau u_{\mathrm{rms}}^2$, so $\tau/(3\mu_0\rho) = B_{\mathrm{eq}}^2/\eta_{\mathrm{t}}$ (see BB02). In fact, the evolution equation for α_{M} is therefore nothing else but the evolution equation for the small scale current helicity, $\overline{\boldsymbol{j} \cdot \boldsymbol{b}}$.

Indeed, $\overline{\boldsymbol{j} \cdot \boldsymbol{b}}$ constitutes a possible source of an α effect, although it occurs usually in conjunction with the kinetic α effect that, in turn, is proportional to the negative kinetic helicity, $\overline{\boldsymbol{\omega} \cdot \boldsymbol{u}}$, where $\boldsymbol{\omega} = \boldsymbol{\nabla} \times \boldsymbol{u}$ is the vorticity. The two effects together tend to diminish the residual α effect. We emphasize, however, that this does not need to be the case, and that even in the absence of kinetic helicity the magnetic α effect needs to be taken into account. One example is the case of a decaying helical large scale magnetic field, where $\overline{\boldsymbol{j} \cdot \boldsymbol{b}}$ is being generated from the large scale field. The associated α_{M} acts as to slow down the decay; see Yousef et al.

(2003) for corresponding simulations, and Blackman & Field (2004) for related model predictions.

The full expression for $\overline{\boldsymbol{\mathcal{E}}}$ can be rather complex. For the present purpose we restrict ourselves to an expression of the form

$$\overline{\boldsymbol{\mathcal{E}}} = (\alpha_{\mathrm{K}} + \alpha_{\mathrm{M}})\overline{\boldsymbol{B}} + \boldsymbol{\delta} \times \overline{\boldsymbol{J}} - \eta_{\mathrm{t}}\overline{\boldsymbol{J}}, \tag{5}$$

where α_{K} is the kinetic α effect, η_{t} is turbulent diffusion, and $\boldsymbol{\delta}$ can represent both Rädler's (1969) $\boldsymbol{\Omega} \times \overline{\boldsymbol{J}}$ effect and the $\overline{\boldsymbol{W}} \times \overline{\boldsymbol{J}}$ or shear–current effect of Rogachevskii & Kleeorin (2003, 2004). (Here $\overline{\boldsymbol{W}} = \boldsymbol{\nabla} \times \overline{\boldsymbol{U}}$ is the vorticity of the mean flow.) The importance of shear, S ($= \partial U_y/\partial x$ in some of the first cases reported blow), and of the two turbulent dynamo effects, α and δ, is quantified in terms of the non-dimensional numbers

$$C_S = \frac{S}{\eta_{\mathrm{t}} k_1^2}, \quad C_\alpha = \frac{\alpha_{\mathrm{K}}}{\eta_{\mathrm{t}} k_1}, \quad C_\delta = \frac{\delta}{\eta_{\mathrm{t}}}. \tag{6}$$

In the following we restrict ourselves to cases where either C_α or C_δ are different from zero.

The general importance of helicity fluxes has been identified by Blackman & Field (2000a,b) and Kleeorin et al. (2000). Here we use a generalized from of the current helicity flux of Vishniac & Cho (2001) flux, as derived by Subramanian & Brandenburg (2004),

$$\overline{\boldsymbol{\mathcal{F}}}_{C\,i}^{\mathrm{SS}} = \phi_{ijk} \overline{B}_j \overline{B}_k. \tag{7}$$

Under the assumption that $\boldsymbol{\nabla} \cdot \overline{\boldsymbol{U}} = 0$, we show in Appendix A that

$$\phi_{ijk} = C_{\mathrm{VC}}\, \epsilon_{ijl} \overline{S}_{lk}, \tag{8}$$

where $\overline{S}_{lk} = \frac{1}{2}(\overline{U}_{l,k} + \overline{U}_{k,l})$ is the mean rate of strain tensor and C_{VC} is a non-dimensional coefficient that is of order unity (see Appendix A). In the following we consider C_{VC} as a free parameter. It turns out that there is a critical value, C_{VC}^*, above which there is runaway growth that can only be stopped by adding an extra quenching term. One possibility is to consider an algebraic quenching of the total α effect ($\alpha = \alpha_{\mathrm{K}} + \alpha_{\mathrm{M}}$). Here we use a rough and qualitative approximation to the full expressions of Kleeorin & Rogachevskii (2002) by using

$$\alpha = \alpha_0 / \left(1 + g_\alpha \overline{\boldsymbol{B}}^2 / B_{\mathrm{eq}}^2 \right), \tag{9}$$

where we choose $g_\alpha = 3$ as a good approximation to the full expression (see BB02 for a discussion in similar context). For a completely independent and purely numerical verification of algebraic and non-R_{m} dependent quenching of α_{K} and α_{M} see Brandenburg & Subramanian (2005b).

We expect the critical value C_{VC}^* to decrease with increasing value of C_S. However, since C_{VC} should normally be fixed by physical considerations (which are uncertain), the possibility of a critical state translates to a critical value of C_S, above which "strong" (or "runaway") dynamo action is possible. This effect is similar to the $\overline{\boldsymbol{W}} \times \overline{\boldsymbol{J}}$ effect in that it only requires nonhelical turbulence and shear. However, we will show that, unless there is also current helicity flux above a certain threshold, the field generated by the $\overline{\boldsymbol{W}} \times \overline{\boldsymbol{J}}$ effect effect alone is weak when there are boundaries and when the magnetic Reynolds number is large. For the same reason, also

α effect dynamos produce only week fields, unless the current helicity flux exceeds a certain threshold.

Once the current helicity flux is supercritical, it is important to make sure that α_{M} is spatially smooth. This is accomplished by adding a small diffusion term of the form $\kappa_\alpha \nabla^2 \alpha_{\mathrm{M}}$ to the right hand side of Eq. (4). (Typical values considered below are $\kappa_\alpha = 0.02 \nu_{\mathrm{t}}$.)

We consider both one-dimensional and two-dimensional models. In both cases we allow for the possibility of shear. In the one-dimensional case ($-L/2 < z < L/2$) we allow for a linear shear flow of the form $\overline{U} = (0, Sx, 0)$, so the mean field dynamo equation is given by

$$\frac{\partial \overline{B}_x}{\partial t} = -\frac{\partial \overline{\mathcal{E}}_y}{\partial z} + \eta \frac{\partial^2 \overline{B}_x}{\partial z^2}, \tag{10}$$

$$\frac{\partial \overline{B}_y}{\partial t} = S\overline{B}_x + \frac{\partial \overline{\mathcal{E}}_x}{\partial z} + \eta \frac{\partial^2 \overline{B}_y}{\partial z^2}, \tag{11}$$

and the current helicity flux is given by

$$\hat{z} \cdot \overline{\mathcal{F}}_C^{\mathrm{SS}} = \tfrac{1}{2} C_{\mathrm{VC}} S(\overline{B}_x^2 - \overline{B}_y^2), \tag{12}$$

where $\hat{z}$ is the unit vector in the z direction. Note that, according to this formula, assuming $S > 0$, and because $\overline{B}_x^2 < \overline{B}_y^2$ in such a shear flow, negative current helicity flows in the positive z direction. This is also the direction of the dynamo wave for $\alpha_{\mathrm{K}} > 0$. [We recall that for $\alpha_{\mathrm{K}} > 0$, negative current helicity must be lost to alleviate catastrophic quenching (Brandenburg et al. 2002).] We assume vacuum boundary conditions,

$$\overline{B}_x = \overline{B}_y = 0 \quad (\text{on } z = \pm L/2), \tag{13}$$

which implies that $\hat{n} \cdot \overline{\mathcal{F}}_C^{\mathrm{SS}} = 0$ on the boundaries. This property can be regarded as an unfortunate shortcoming of the present model, because, although current helicity can efficiently be transported to the vicinity of the boundary, it is actually unable to leave the domain. On the other hand, this type of boundary condition was also used in the simulations presented in Brandenburg (2005, hereafter referred to as B05) where the absence of closed boundaries clearly did allow for a significantly enhanced final field strength (see also Brandenburg et al. 2005). (It is also possible that in the simulations current helicity of the small scale field got lost because of numerical dissipation on the boundaries.)

In order to allow for a finite current helicity flux on the boundaries we also compare with the case of an extrapolating boundary condition,

$$\epsilon z \frac{\partial \overline{B}_i}{\partial z} + \overline{B}_i = 0 \quad (\text{on } z = \pm L/2 \text{ for } i = x, y). \tag{14}$$

Thus, if $\epsilon = 0$ we recover the standard vacuum boundary condition, $\overline{B}_i = 0$. For $\epsilon > 0$, the slope of $\overline{B}_i(z)$ is such that $\overline{B}_i$ would vanish outside the domain on fiducial reference points, $z = \pm(1 + \epsilon)L/2$.

In the two-dimensional simulations we consider two different cases. In the first case we use Eq. (13) in the vertical direction and periodic boundary conditions in the horizontal. In the second case we use perfectly conducting and pseudo-vacuum boundary conditions on the four boundaries in a meridional cross-section, just like in the corresponding direct simulations (BS04). The pseudo-vacuum boundary

conditions are applied on what would correspond in the sun to the outer surface and the equatorial plane.

In all cases the initial magnetic field is a random field of sufficiently small amplitude, so that the nonlinear solutions grow out of the linear one. We have not made a serious attempt to search for solutions that only exist as finite amplitude solutions. Furthermore, we assume that initially $\alpha_{\mathrm{M}} = 0$, which is sensible if one starts with weak initial fields. Again, we have not made a systematic search for finite amplitude solutions that might only be accessible with finite initial values of α_{M}.

3. Results

3.1. Reference case with no shear

We begin with the case of an α^2 dynamo where $S = 0$, so there is no shear and hence no helicity flux. The dynamo is excited for $\alpha > \eta_{\mathrm{T}} k_1$. A possible solution that is marginally excited and satisfies the boundary condition (13) is given by

$$\overline{B}(z) = \begin{pmatrix} 1 + \cos k_1 z \\ -\sin k_1 z \\ 0 \end{pmatrix}; \tag{15}$$

see Meinel & Brandenburg (1990) for the more general case of non-marginally excited (but still only kinematic) solutions.

We have solved Eqs. (10) and (11) numerically using a third-order Runge-Kutta time stepping scheme and a sixth-order finite difference scheme. An example of a solution is shown in Fig. 1. The results are displayed in Table 1 and Fig. 2. Both simulation data and mean field models are roughly compatible with the relation

$$\langle \overline{B}^2 \rangle / B_{\mathrm{eq}}^2 \propto R_{\mathrm{m}}^{-1} \quad (\text{with boundaries}), \tag{16}$$

that was first found analytically by Gruzinov & Diamond (1995) for the same boundary conditions (13). The simulation data shown in Fig. 2 supersede earlier results of Brandenburg & Dobler (2001) at lower resolution and smaller values of R_{m} where the scaling seemed compatible with $\overline{B}^2 \sim R_{\mathrm{m}}^{-1/2}$. However, in view of the new results this must now be regarded as an artifact of insufficient dynamical range, so the correct scaling is given by Eq. (16). Furthermore, the simulation results give agreement with the mean field model if the dynamo number, C_α, is somewhere between 3 and 10. This appears compatible with the fact that the scale separation ratio in the simulation is $k_{\mathrm{f}}/k_1 = 5$, and that this ratio gives a good estimate of C_α; see BB02.

Returning now to the description of the mean field calculations, we note that at large values of R_{m} the system shows relaxation oscillations where the sign of the field does not necessarily change (so the period of the field agrees with the period of the rms value). The frequency given in the table is $\omega = 2\pi/T_{\mathrm{period}}$.

The fact that the saturation field strength decreases with increasing magnetic Reynolds number is bad news for astrophysical applications. However, this result is in agreement with simulations, lending thereby support to the applicability of mean field theory.
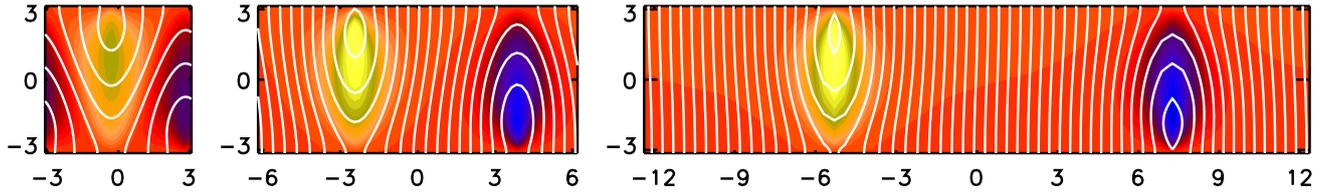
Fig. 3. (online colour at www.an-journal.org) Field lines superimposed on a color/gray scale representation of the normal field component for an α^2 dynamo in two dimensions in the xz plane with $C_\alpha = 3$ and three different aspect ratios (1, 2, and 4). Note that there remain only two cells even for large aspect ratios.
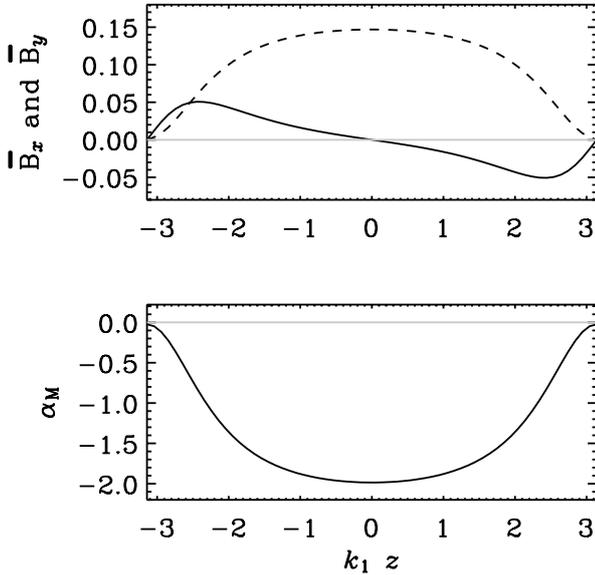

Fig. 1. Field structure for an α^2 dynamo (solid line $\overline{B}_x/B_{\rm eq}$, dashed line $\overline{B}_y/B_{\rm eq}$) together with $\alpha_{\rm M}$, for $C_\alpha = 3$, and $R_{\rm m} = 10^2$.
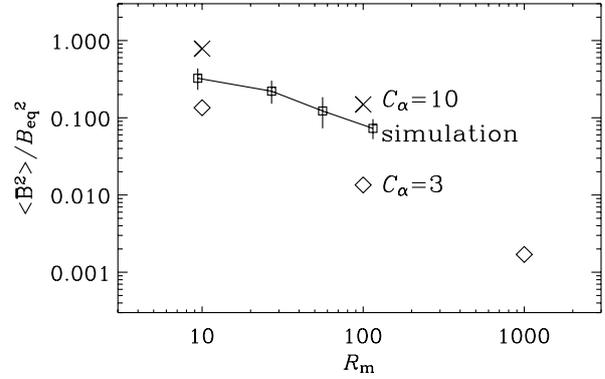

Fig. 2. Dependence of $\langle\overline{\boldsymbol{B}}^2\rangle/B_{\rm eq}^2$ on the magnetic Reynolds number for a run with open boundary conditions and no shear both for the mean field model and the direct simulation (squares connected by a line, with approximate error bars). The diamonds and crosses refer to mean field models where C_α is 3 and 10, respectively.

main in that direction (Fig. 3), and the field amplitude still decreases inversely proportional to the magnetic Reynolds number (Table 2).

3.2. Solutions with uniform shear

For positive values of $\alpha_{\rm K}$ and positive values of S there are dynamo waves traveling in the positive z direction. This is also the direction in which the flux of negative current helicity is pointing. Note that the saturation magnetic field strength decreases with increasing magnetic Reynolds number in the same way as before (Table 3). The modified boundary condi-

The situation may change by allowing the field to extend also in one of the perpendicular directions (say the x direction), because then the field may have its main variation in this new direction. In particular, if the field were to display Beltrami-like behavior in that direction, it might be more similar to the case of triply periodic boundary conditions. However, as can be seen from Table 2, this does not seem to be the case. Even at large aspect ratios the wavelength of the field in the x direction remains of the order of the extent of the do-

Table 1. Mean squared field strength of dynamically quenched α^2 dynamos. For time dependent solutions $\overline{B}^2$ is also averaged in time, and the frequency of the solution is given. Note in particular the inverse proportionality between $\langle\overline{\boldsymbol{B}}^2\rangle$ and $R_{\rm m}$ in the first three rows (marked by asterisks).

	$R_{\rm m}$	C_α	$\langle\overline{\boldsymbol{B}}^2\rangle/B_{\rm eq}^2$	$\omega/(\eta_{\rm T}k_1^2)$
*	10^1	3	1.35×10^{-1}	0
*	10^2	3	1.35×10^{-2}	0
*	10^3	3	1.74×10^{-3}	0.28
	10^1	10	7.85×10^{-1}	0.85
	10^2	10	1.49×10^{-1}	0.64

Table 2. Same as in Table 1, but for two-dimensional calculations for different values of $R_{\rm m}$ and different aspect ratios L_x/L_z. The inverse proportionality between $\langle\overline{\boldsymbol{B}}^2\rangle$ and $R_{\rm m}$ can best be seen from the last three rows (marked by asterisks). The effect of changing the aspect ratio can be seen by inspecting the first two and the fourth row.

	$R_{\rm m}$	C_α	L_x/L_z	$\langle\overline{\boldsymbol{B}}^2\rangle/B_{\rm eq}^2$	$\omega/(\eta_{\rm T}k_1^2)$
	10^2	3	1	1.06×10^{-1}	0
	10^2	3	2	2.30×10^{-1}	0
*	10^1	3	4	1.25×10^{-0}	0
*	10^2	3	4	2.53×10^{-1}	0
*	10^3	3	4	2.71×10^{-2}	0

tion (14) with $\epsilon \neq 0$ does lead to an increase of the saturation field strength for $R_\mathrm{m} = 10^2$, but not for $R_\mathrm{m} = 10^3$. This behavior is not altered by the presence of helicity fluxes, i.e. changing the value of C_VC from 0 to 0.2 has only a small effect.

For $C_S = 10$, the critical value for runaway dynamo action is $C_\mathrm{VC}^* = 0.15$, but it decreases with increasing shear (e.g. for $C_S = 20$ we have $C_\mathrm{VC}^* = 0.036$.) This runaway growth may be a possible solution to the quenching problem in that it allows the solution to continue growing until it is saturated by other effects such as the usual α quenching that is independent of R_m; see Eq. (9). Note that when runaway occurs, the magnetic field increases sharply until it reaches a new saturation value close to equipartition; see Fig. 4, where $C_\mathrm{VC} = 1$ has been chosen. However, the magnetic field is then no longer oscillatory. Obviously, the algebraic quenching adopted here is not realistic, but it does at least illustrate the point that when C_VC exceeds a certain critical value, there is runaway that could potentially be contained by having additional quenching terms.

As was already anticipated by Vishniac & Cho (2001), a supercritical current helicity flux could by itself also drive a mean field dynamo. This mechanism requires a finite amplitude initial magnetic field to get started; see Fig. 5. With unsuitable initial conditions the dynamo may therefore not get started and one might miss it. It is also possible that, even though the expected helicity flux is present and of the right kind, its strength remains subcritical (Arlt & Brandenburg 2001).

It is interesting to note that much of the late kinematic phase does not depend on the value of R_m; see Fig. 6. In fact, during the kinematic phase the runs with larger values of R_m have slightly larger magnetic energies. Within a time scale that is independent of R_m [here 2000 dynamical time

Table 3. Mean squared field strength of dynamically quenched $\alpha^2\Omega$ dynamos. For time dependent solutions $\overline{\boldsymbol{B}}^2$ is also averaged in time, and the frequency of the solution is given. For all calculations we used 64 meshpoints. For $C_\alpha = 0.2$ and $C_S = 10$ the kinematic growth rate is 0.08. The inverse proportionality between $\langle\overline{\boldsymbol{B}}^2\rangle$ and R_m can best be seen from the first three rows (marked by asterisks). Changing the sign of C_S has no effect on the saturation field strengths, regardless of the value of C_VC.

	R_m	ϵ	C_VC	$\langle\overline{\boldsymbol{B}}^2\rangle/B_\mathrm{eq}^2$	$\omega/(\eta_\mathrm{T}k_1^2)$
*	10^1	0	0	1.52×10^{-2}	0.53
*	10^2	0	0	1.49×10^{-3}	0.56
*	10^3	0	0	2.49×10^{-4}	0.54
	10^1	0	0.2	3.18×10^{-2}	0.44
	10^2	0	0.2	1.57×10^{-3}	0.57
	10^1	0	-0.2	1.06×10^{-2}	0.56
	10^2	0	-0.2	1.35×10^{-3}	0.57
	10^1	0.2	0	3.58×10^{-3}	0.59
	10^2	0.2	0	7.73×10^{-2}	0.36
	10^1	0.2	0.2	4.31×10^{-3}	0.58
	10^2	0.2	0.2	1.45×10^{-2}	0.22
	10^3	0.2	0.2	4.26×10^{-4}	0.47

Fig. 4. Evolution of $\langle\overline{\boldsymbol{B}}^2\rangle/B_\mathrm{eq}^2$ for a model with $C_\mathrm{VC} = 1$ and additional algebraic quenching with $g_\alpha = 3$, $\kappa_\alpha = 0.02\eta_\mathrm{t}$, $C_S = 10$, $C_\alpha = 0.2$, and $R_\mathrm{m} = 10^4$. Note that the abscissa is scaled in resistive time units.
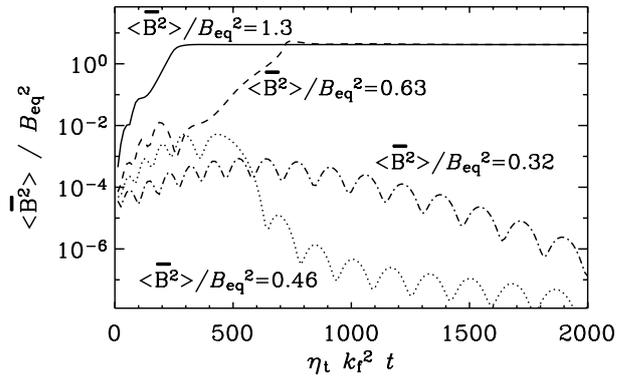

Fig. 5. Evolution of $\langle\overline{\boldsymbol{B}}^2\rangle/B_\mathrm{eq}^2$ of dynamo with no kinetic helicity $C_\alpha = 0$, just shear with $C_S = 10$ and a supercritical current helicity flux with $C_\mathrm{VC} = 1$, and different initial field strengths. (Because the initial field is random, much of the initial energy is lost by dissipation in the high wavenumbers.) In all cases $R_\mathrm{m} = 10^4$. Note that the abscissa is scaled in dynamical time units.
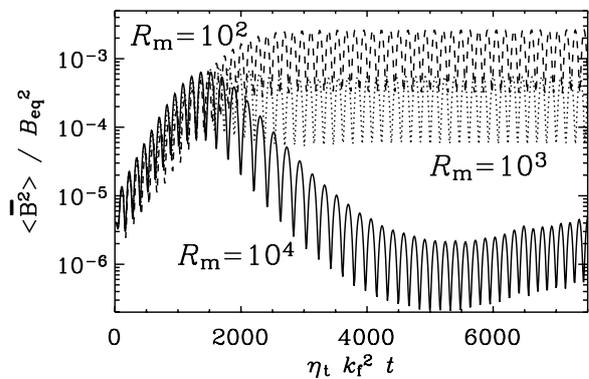

Fig. 6. Evolution of $\langle\overline{\boldsymbol{B}}^2\rangle/B_\mathrm{eq}^2$ for the $\alpha^2\Omega$ dynamo with $C_\alpha = 0.2$, $C_S = 10$, $C_\mathrm{VC} = 0.2$, and different values of R_m. Note that the abscissa is scaled in dynamical time units.
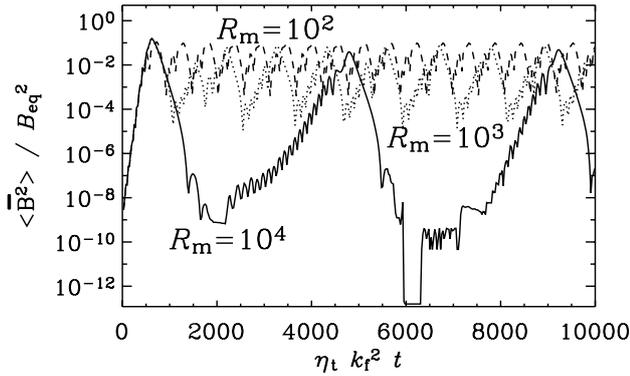
Fig. 7. Evolution of $\langle \overline{\boldsymbol{B}}^2 \rangle / B_{\mathrm{eq}}^2$ for the $\alpha^2\Omega$ dynamo with $C_\alpha = 0.2$, $C_S = 30$, $C_{\mathrm{VC}} = 0$, and different values of R_{m}. The line styles are as in Fig. 6 above.

units, $(\eta_t k_{\mathrm{f}}^2)^{-1}$] the large scale magnetic energy reaches a significant field strength whose peak value is roughly independent of the magnetic Reynolds number. If one discards the subsequent decline of the magnetic energy, this result would be similar to that in the homogeneous case. In the weakly supercritical case, the cycle frequency does not decrease as nonlinearity becomes important. This is indeed an important feature of the dynamical quenching model that distinguishes it from the catastrophic quenching hypothesis (BB02). The run presented in Fig. 6 is for a finite current helicity flux ($C_{\mathrm{VC}} = 0.2$), but the qualitative form of this plot is actually independent of helicity fluxes and can also be obtained for $C_{\mathrm{VC}} = 0$, for example.

If the dynamo number is increased further to be highly supercritical then the peak value reached by the large scale field, at the end of the late kinematic stage, increases even further; see Fig. 7. This is again as anticipated by BB02 and Subramanian (2002). However, what was not anticipated are the subsequent strong dips in the mean field energy. It appears that the growth of α_{M} and the subsequent decrease of α, takes the dynamo below criticality. The mean field then decays until the microscopic diffusivity term [last term in Eq. (4)] causes α_{M} to decay on a resistive timescale, and the net α to again increase, such that the dynamo becomes supercritical again. This qualitatively accounts for the long term oscillations of the mean field energy seen in Fig. 7, whose period clearly increases with R_{m}. It however implies that, on the average, the mean field energy again decreases with increasing R_{m}, when there is no flux.

3.3. Shear-current effect

The issue of catastrophic quenching is often associated with the α effect alone, and it is implied that other large scale dynamo effects may not have this problem. This is however not true. The main problem is quite generally associated with the helical nature of the large scale magnetic field. As is well known, the $\overline{\boldsymbol{W}} \times \overline{\boldsymbol{J}}$ effect can exist even without kinetic helicity and just shear alone (Rogachevskii & Kleeorin 2003, 2004). In the presence of closed boundaries, the current helicity of the large scale field results in a corresponding contri-
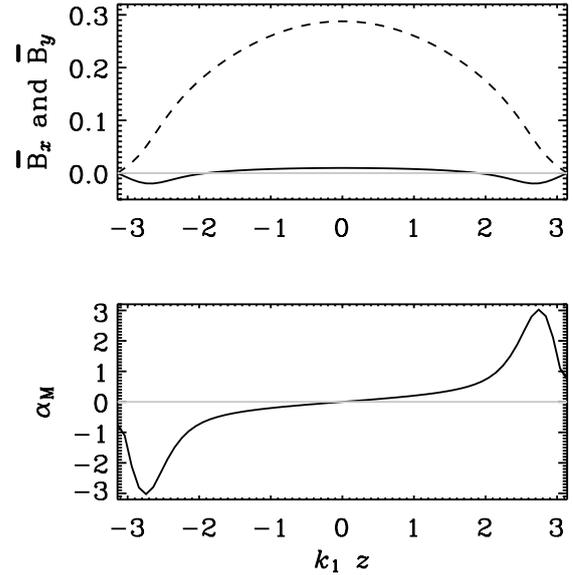

Fig. 8. Field structure for a $\boldsymbol{\delta} \times \overline{\boldsymbol{J}}$ dynamo (solid line $\overline{B}_x/B_{\mathrm{eq}}$, dashed line $\overline{B}_y/B_{\mathrm{eq}}$) together with α_{M}, for $C_\delta = -1$, $C_S = 2$, $C_{\mathrm{VC}} = 2$, and $R_{\mathrm{m}} = 10^3$.

bution from the small scale field, which affects the resulting electromotive force. This can be seen quite generally by considering the stationary limit of Eq. (4) for the case $C_{\mathrm{VC}} = 0$, which yields $\alpha_{\mathrm{M}} = -R_{\mathrm{m}}\overline{\boldsymbol{\mathcal{E}}} \cdot \overline{\boldsymbol{B}}/B_{\mathrm{eq}}^2$,

$$\overline{\boldsymbol{\mathcal{E}}} \cdot \overline{\boldsymbol{B}} = \frac{\overline{\boldsymbol{\mathcal{E}}}_0 \cdot \overline{\boldsymbol{B}}}{1 + R_{\mathrm{m}}\overline{\boldsymbol{B}}^2/B_{\mathrm{eq}}^2} \quad \text{(steady state)}. \tag{17}$$

Here we have defined the unquenched electromotive force

$$\overline{\boldsymbol{\mathcal{E}}}_0 = \alpha_{\mathrm{K}}\overline{\boldsymbol{B}} + \boldsymbol{\delta} \times \overline{\boldsymbol{J}} - \eta_t\overline{\boldsymbol{J}}, \tag{18}$$

where the α_{M} term is absent compared with Eq. (5). To illustrate the catastrophic quenching of the $\overline{\boldsymbol{W}} \times \overline{\boldsymbol{J}}$ effect we set $\alpha_{\mathrm{K}} = 0$ and $\boldsymbol{\delta} = (0, 0, \delta)^{\mathrm{T}}$.

As is already clear from linear theory, a $\boldsymbol{\delta} \times \overline{\boldsymbol{J}}$ effect can only produce self-excited solutions if $\delta/S < 0$ (e.g. Brandenburg & Subramanian 2005a), where the shear associated with $\overline{\boldsymbol{W}}$ is responsible for stretching the poloidal field into toroidal. The $\boldsymbol{\delta} \times \overline{\boldsymbol{J}}$ effect can also convert poloidal field into toroidal field, in addition to converting toroidal into poloidal, but this effect alone would not produce energy in the mean magnetic field. This is why shear is necessary. [We note, however, that there is currently a controversy regarding the expected sign of the $\boldsymbol{\delta} \times \overline{\boldsymbol{J}}$ effect; see Rüdiger & Kitchatinov (2005).]

The field geometry is shown in Fig. 8; it resembles that of an α^2 dynamo (cf. Fig. 1), except that now both B_x and B_y are symmetric about the midplane, and α_{M} is antisymmetric about $z = 0$. (The symmetry property of α_{M} is identical to that of $\overline{\boldsymbol{\mathcal{E}}} \cdot \overline{\boldsymbol{B}}$, where one contribution is $(\boldsymbol{\delta} \times \overline{\boldsymbol{J}}) \cdot \overline{\boldsymbol{B}} = \frac{1}{2}\boldsymbol{\delta} \cdot \nabla\overline{\boldsymbol{B}}^2$.) In Table 4 we present the results for different values of R_{m}. Again, we see quite unambiguously that, for a fixed value of S, the resulting field strength decreases with increasing R_{m}, just like in all previous cases.

Table 4. Mean squared field strength of dynamically quenched $\delta^2\Omega$ dynamos. For all calculations we used 64 meshpoints. The inverse proportionality between $\langle\overline{\boldsymbol{B}}^2\rangle$ and R_{m} can again be seen from the last two rows (marked by asterisks).

	R_{m}	C_δ	C_S	C_{VC}	$\langle\overline{\boldsymbol{B}}^2\rangle/B_{\mathrm{eq}}^2$	$\omega/(\eta_{\mathrm{T}}k_1^2)$
	10^2	-1.0	2	0	1.48×10^{-1}	0
	10^2	-1.0	2	1	2.21×10^{-1}	0
*	10^2	-1.0	2	2	4.24×10^{-1}	0
*	10^3	-1.0	2	2	4.39×10^{-2}	0
*	10^4	-1.0	2	2	4.16×10^{-3}	0

3.4. Solar-like shear

Finally, we consider the more complex flow geometry employed by BS04 and B05 in an attempt to approximate the differential rotation profile in lower latitudes of the sun (cf. Figs 1 and 2 of BS04). In the simulations presented in these two papers the turbulence was forced in such a way that it has either positive, negative, or zero kinetic helicity. The latter case would correspond to no α effect, but the $\overline{\boldsymbol{W}}\times\overline{\boldsymbol{J}}$ effect may still provide a possible explanation for the large scale field that is actually generated in such a simulation (B05).

We use here the solar-like shear profile of BS04 that is given by

$$\overline{\boldsymbol{U}} = (S/k_1)(0, \cos k_1 x \, \cos k_1 z, 0)^{\mathrm{T}} \qquad (19)$$

in the domain $-\pi/2 \le k_1 x \le 0$, $0 \le k_1 z \le \pi/2$. As discussed in BS04, $k_1 x = -\pi/2$ corresponds to the bottom of the convection zone, where the toroidal flow is constant and approximately equal to that at 30 degrees latitude (corresponding to $k_1 z = \pi/2$; the surfaces at $z = 0$ and $x = 0$ correspond to equator and outer surface, respectively, and permit current helicity fluxes.

Length is measured in units of the inverse basic wavenumber of the domain, k_1^{-1}. Hereafter we assume $k_1 = 1$. The rate of strain matrix is then given by

$$\overline{\mathsf{S}} = -\tfrac{1}{2}S \begin{pmatrix} 0 & \sin x \cos z & 0 \\ \sin x \cos z & 0 & \cos x \sin z \\ 0 & \cos x \sin z & 0 \end{pmatrix}, \quad (20)$$

so the divergence of the current helicity flux is, using Eqs. (7) and (8), given by

$$\frac{\boldsymbol{\nabla}\cdot\overline{\boldsymbol{\mathcal{F}}}_C^{\mathrm{SS}}}{\tfrac{1}{2}SC_{\mathrm{VC}}} = -\cos x \, \sin z\left[\frac{\partial}{\partial x}\left(\overline{B}_y^2 - \overline{B}_z^2\right) + \frac{\partial}{\partial z}\left(\overline{B}_x\overline{B}_z\right)\right]$$
$$+ \sin x \, \cos z\left[\frac{\partial}{\partial z}\left(\overline{B}_y^2 - \overline{B}_x^2\right) + \frac{\partial}{\partial x}\left(\overline{B}_x\overline{B}_z\right)\right]$$
$$+ \sin x \, \sin z\left(\overline{B}_x^2 - \overline{B}_z^2\right). \qquad (21)$$

The corresponding value of $\boldsymbol{\nabla}\cdot\overline{\boldsymbol{\mathcal{F}}}_C^{\mathrm{SS}}$ is used in Eq. (4), and the dynamo equation (3) is solved subject to the same boundary conditions used in BS04.

The field turns out to be highly irregular in time. An example of a snapshot at an arbitrarily chosen moment in time is given in Fig. 9. The magnetic field looks roughly similar to that found by averaging the results of direct simulations; see Fig. 6 of B05 or Fig. 18 of Brandenburg et al. (2005).
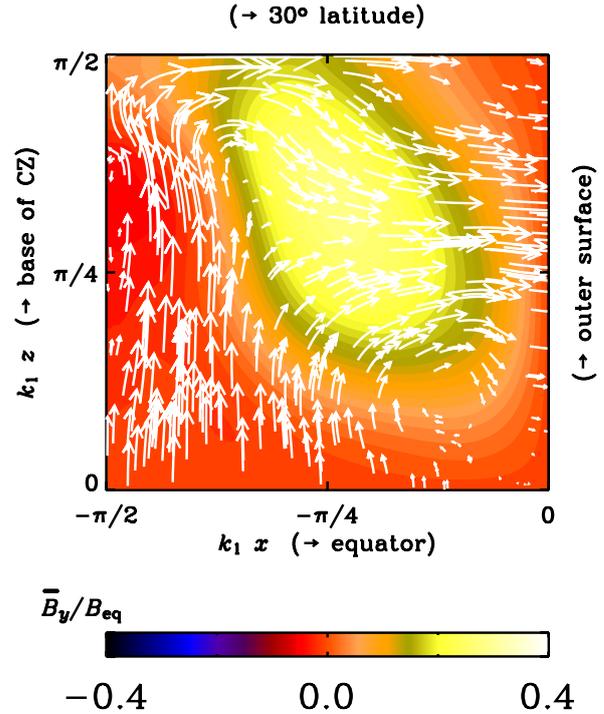

$\overline{B}_y/B_{\mathrm{eq}}$

$-0.4 \qquad 0.0 \qquad 0.4$

Fig. 9. (online colour at www.an-journal.org) Snapshot showing the field structure for an $\alpha^2\Omega$ dynamo with solar-like shear, $C_\alpha = 3$, $C_S = 10^3$, $C_{\mathrm{VC}} = 10^{-3}$, and $R_{\mathrm{m}} = 10^2$. The solution remains highly time-dependent.

Table 5. Mean squared field strength of dynamically quenched $\alpha^2\Omega$ dynamos with a solar-like shear profile. All solutions are time dependent, so $\overline{\boldsymbol{B}}^2$ is also averaged in time, and the frequency of the field (not its energy) is given. The inverse proportionality between $\langle\overline{\boldsymbol{B}}^2\rangle$ and R_{m} can be seen from the first three rows (marked by asterisks). For all calculations we used 128^2 meshpoints using $C_\alpha = 3$ and $C_S = 10^3$.

	R_{m}	C_α	C_S	C_{VC}	$\langle\overline{\boldsymbol{B}}^2\rangle/B_{\mathrm{eq}}^2$
*	10^1	3	10^3	0.1	9.4×10^{-2}
*	10^2	3	10^3	0.1	9.2×10^{-3}
*	10^3	3	10^3	0.1	8.4×10^{-4}
	10^2	3	10^3	0.001	2.96×10^{-1}
	10^2	3	10^3	0.01	4.98×10^{-2}
	10^2	3	10^3	0.1	9.22×10^{-3}

In Table 5 we give the time and volume averaged values of the squared mean field for different values of R_{m} and different values of C_{VC}. Again, note that the energy of the mean field decreases inversely proportional to the magnetic Reynolds number. More surprisingly, increasing the value of C_{VC} has an adverse effect on the saturation field amplitude.

4. Conclusions

The present investigations still leave us with a puzzle. On the one hand the dynamically quenched mean field models yield

invariably a resistively quenched saturation amplitude of the mean field – regardless of details of the boundary conditions, the presence of shear, or the nature of the dynamo effect. (In the absence of shear and just α^2 dynamo action, this result of mean field theory is well confirmed by turbulence simulations.) On the other hand, simulations with open boundary conditions (B05) have shown a clear difference compared with the case of closed boundaries. The reason for this discrepancy remains unclear at this point. It is however possible that C_{VC} is simply large enough, so there is a runaway dynamo effect driving large scale fields by the Vishniac & Cho mechanism. A possible argument against this explanation, is that in B05, the dynamo did not resemble threshold behavior.

Even though for subcritical helicity fluxes the saturation field strength may decrease with increasing R_{m}, the field strength at the end of the kinematic regime seems to be still independent of R_{m}. This is at least qualitatively similar to the behavior of homogeneous dynamos (BB02; Subramanian 2002). Furthermore, the peak field strength at the end of the kinematic phase depends on the strength of the dynamo number, which is also similar to what is predicted based on homogeneous dynamo theory (cf. Subramanian 2002; Brandenburg & Subramanian 2005a).

Clearly, further investigations of current helicity fluxes are warranted to pin down the origin of the apparently unquenched saturation amplitude of the simulations. It was already noted by BS04 that the Vishniac & Cho flux only accounted for about one quarter of the total current helicity flux that was determined from the simulations. This could also indicate that another perhaps more important component still needs to be included in the present mean field models. It is possible that the helicity fluxes discussed by Kleeorin et al. (2000, 2002, 2003a,b) may capture the missing components of the helicity flux, but this remains at this point only speculation.

The present work has shown that there is a threshold of the current helicity flux above which runaway-type dynamo action is possible. It remains a challenge to determine whether in fact all existing high magnetic Reynolds number dynamos lie in this very same regime. Clearly, more work is needed to establish whether existing large scale dynamos without kinetic helicity and just shear (B05) operate in this supercritical helicity flux regime by the Vishniac & Cho mechanism, or whether they work with the shear–current effect, for example.

References

Arlt, R., Brandenburg, A.: 2001, A&A 380, 359
Blackman, E.G., Field, G.B.: 2000, ApJ 534, 984
Blackman, E.G., Field, G.B.: 2000, MNRAS 318, 724
Blackman, E.G., Field, G.B.: 2004, PhPl 11, 3264
Blackman, E.G., Brandenburg, A.: 2002, ApJ 579, 359 (BB02)
Brandenburg, A.: 2001, ApJ 550, 824 (B01)
Brandenburg, A.: 2005, ApJ 625, 539 (B05)
Brandenburg, A., Dobler, W.: 2001, A&A 369, 329
Brandenburg, A., Sandin, C.: 2004, A&A 427, 13 (BS04)
Brandenburg, A., Subramanian, K.: 2005a, PhR [arXiv: astro-ph/0405052]
Brandenburg, A., Subramanian, K.: 2005b, A&A [arXiv: astro-ph/0504222]
Brandenburg, A., Dobler, W., Subramanian, K.: 2002, AN 323, 99
Brandenburg, A., Haugen, N.E.L., Käpylä, P.J., Sandin, C.: 2005, AN 326, 174
Field, G.B., Blackman, E.G.: 2002, ApJ 572, 685
Gruzinov, A.V., Diamond, P.H.: 1994, PhRvL 72, 1651
Gruzinov, A.V., Diamond, P.H.: 1995, PhPl 2, 1941
Kleeorin, N.I., Ruzmaikin, A.A.: 1982, Magnetohydrodynamics 18, 116
Kleeorin, N., Rogachevskii, I., Ruzmaikin, A.: 1995, A&A 297, 159
Kleeorin, N., Moss, D., Rogachevskii, I., Sokoloff, D.: 2000, A&A 361, L5
Kleeorin, N., Moss, D., Rogachevskii, I., Sokoloff, D.: 2002, A&A 387, 453
Kleeorin, N., Moss, D., Rogachevskii, I., Sokoloff, D.: 2003a, A&A 400, 9
Kleeorin, N., Kuzanyan, K., Moss, D., Rogachevskii, I., Sokoloff, D., Zhang, H.: 2003b, A&A 409, 1097
Meinel, R., Brandenburg, A.: 1990, A&A 238, 369
Rädler, K.-H.: 1969, Geod. Geophys. Veröff., Reihe II 13, 131
Roberts, P.H., Soward, A.M.: 1975, AN 296, 49
Rogachevskii, I., Kleeorin, N.: 2003, PhRvE 68, 036301
Rogachevskii, I., Kleeorin, N.: 2004, PhRvE 70, 046310
Rüdiger, G., Kitchatinov, L.L.: 2005, PhRvE, submitted
Subramanian, K.: 2002, BASI 30, 715
Subramanian, K., Brandenburg, A.: 2004, PhRvL 93, 205001
Vishniac, E.T., Cho, J.: 2001, ApJ 550, 752
Yousef, T.A., Brandenburg, A., Rüdiger, G.: 2003, A&A 411, 321

Appendix A: Vishniac-Cho flux in a shear flow

We derive here the form of the Vishniac-Cho flux, introduced in Eq. (7), assuming that the underlying turbulence is homogeneous and isotropic (and weakly or not helical), and that all the anisotropy required to get a non-zero ϕ_{ijk} arises from the influence of large scale velocity shear. We use the two-scale approach of Roberts & Soward (1975) whereby one assumes that the correlation tensor of fluctuating quantities ($\boldsymbol{u}$ and $\boldsymbol{b}$) vary slowly on the system scale, say $\boldsymbol{R}$. From Subramanian & Brandenburg (2004) we have

$$\phi_{spk} = -4\tau\epsilon_{klm}\int k_l k_p v_{ms}(\boldsymbol{k},\boldsymbol{R})\,\mathrm{d}^3 k, \tag{A1}$$

where

$$v_{ms} = \int \overline{\hat{u}_m(\boldsymbol{k}+\tfrac{1}{2}\boldsymbol{K})\hat{u}_s(-\boldsymbol{k}+\tfrac{1}{2}\boldsymbol{K})}.\mathrm{e}^{\mathrm{i}\boldsymbol{K}\cdot\boldsymbol{R}}\,\mathrm{d}^3 K. \tag{A2}$$

Here $\hat{u}_m$ is the Fourier transform of the velocity component u_m. Note that for homogeneous isotropic turbulence ϕ_{spk} vanishes. Now suppose we consider the effect of a weak shear on this turbulence. Then one can approximate its effect as giving an extra first order contribution to the velocity, $\boldsymbol{u} = \boldsymbol{u}^{(0)} + \boldsymbol{u}^{(1)}$, where $\boldsymbol{u}^{(0)}$ is the isotropic homogeneous part. From the perturbed momentum equation, $\boldsymbol{u}^{(1)} \approx -\tau_*[\boldsymbol{u}^{(0)}\cdot\boldsymbol{\nabla}\overline{\boldsymbol{U}} + \overline{\boldsymbol{U}}\cdot\boldsymbol{\nabla}\boldsymbol{u}^{(0)} - \boldsymbol{\nabla}p]$. Here p is the perturbed pressure which ensures $\boldsymbol{\nabla}\cdot\boldsymbol{u}^{(1)} = 0$, and τ_* is some relaxation time. In Fourier space one can then write

$$\hat{u}_m^{(1)}(\boldsymbol{k}) = -\tau_* P_{mj}(\boldsymbol{k})\int \left[\mathrm{i}k_q'\hat{u}_q^{(0)}(\boldsymbol{k}-\boldsymbol{k}')\overline{\hat{U}}_j(\boldsymbol{k}')\right.$$
$$\left. + \mathrm{i}(k_q-k_q')\hat{u}_j^{(0)}(\boldsymbol{k}-\boldsymbol{k}')\overline{\hat{U}}_q(\boldsymbol{k}')\right]\mathrm{d}^3 k', \tag{A3}$$

where $P_{mj}(\boldsymbol{k}) = \delta_{mj} - k_m k_j / k^2$ is the projection operator which ensures the incompressibility condition on $\boldsymbol{u}^{(1)}$. Also $\hat{\overline{U}}_q$ is the Fourier transform of $\overline{U}_q$.

We now substitute $\boldsymbol{u} = \boldsymbol{u}^{(0)} + \boldsymbol{u}^{(1)}$ in Eqs. (A1) and (A2), keeping only terms linear in $\boldsymbol{u}^{(1)}$. Let us denote the two terms on the RHS of Eq. (A3) as $\hat{u}_s^{(1a)}$ and $\hat{u}_s^{(1b)}$. Then on substituting Eq. (A3) into Eq. (A1), Eq. (A2), four terms result, schematically of the form, Term I: $\hat{u}_m^{(0)} \hat{u}_s^{(1a)}$, Term II: $\hat{u}_m^{(1a)} \hat{u}_s^{(0)}$, Term III: $\hat{u}_m^{(0)} \hat{u}_s^{(1b)}$, Term IV: $\hat{u}_m^{(1b)} \hat{u}_s^{(0)}$. The simplification of these terms involve tedious algebra. We outline the steps for Term I and simply quote the results for other terms. Term I is given by

$$
\begin{aligned}
\phi_{skp}^{\mathrm{I}} = {} & 4\tau\tau_* \epsilon_{klm} \int \Big[k_l k_p P_{mj}(\boldsymbol{k} + \boldsymbol{K}/2)\, \mathrm{i}k_q' \mathrm{e}^{\mathrm{i}\boldsymbol{K}\cdot\boldsymbol{R}} \hat{\overline{U}}_j(\boldsymbol{k}') \\
& \times \overline{\hat{u}_q^{(0)}(\boldsymbol{k} + \tfrac{1}{2}\boldsymbol{K} - \boldsymbol{k}')\hat{u}_s^{(0)}(-\boldsymbol{k} + \tfrac{1}{2}\boldsymbol{K})} \Big]\, \mathrm{d}^3 K\, \mathrm{d}^3 k\, \mathrm{d}^3 k'. \quad \text{(A4)}
\end{aligned}
$$

We change variables to $\boldsymbol{K}' = \boldsymbol{K} - \boldsymbol{k}'$ and integrate over $\boldsymbol{K}'$, keeping in mind that the zeroth order $\boldsymbol{u}^{(0)}$ is homogeneous. Also, since $\overline{U}$ only varies slowly with $\boldsymbol{R}$, we retain only up to first derivative in $\overline{U}$, which implies retaining only terms linear in $\boldsymbol{k}'$ in the above integrals. One then has on evaluating the $\boldsymbol{K}'$ and $\boldsymbol{k}'$ integrals

$$
\begin{aligned}
\phi_{skp}^{\mathrm{I}} = {} & 4\tau\tau_* \epsilon_{klm} \boldsymbol{\nabla}_q \overline{U}_m \int k_l k_p v_{qs}^{(0)} \mathrm{d}^3 k \\
= {} & -\frac{4\tau\tau_* \mathcal{A}}{15} \Big[\epsilon_{ksm} \boldsymbol{\nabla}_p \overline{U}_m + \epsilon_{klm} \boldsymbol{\nabla}_l \overline{U}_m \delta_{ps} \Big]. \quad \text{(A5)}
\end{aligned}
$$

Here we have taken the kinetic energy spectrum for the homogeneous part of the turbulence to be $v_{qs}^{(0)} = P_{qs}(\boldsymbol{k})E(k)$, and done the angular integrals over $\boldsymbol{k}$ space. Also $\mathcal{A} = \int E(k)k^2 \mathrm{d}^3 k$. Similarly we get for Term II:

$$
\phi_{skp}^{\mathrm{II}} = -\frac{4\tau\tau_* \mathcal{A}}{15} \Big[\epsilon_{ksm} \boldsymbol{\nabla}_m \overline{U}_p + \epsilon_{klm} \boldsymbol{\nabla}_m \overline{U}_l \delta_{ps} \Big] \quad \text{(A6)}
$$

and so $\phi_{skp}^{\mathrm{I}} + \phi_{skp}^{\mathrm{II}} = (8\tau\tau_* \mathcal{A}/15)\, \epsilon_{skm} \overline{\mathsf{S}}_{mp}$. A similar calculation can be done for Terms III and IV to get $\phi_{skp}^{\mathrm{III}} + \phi_{skp}^{\mathrm{IV}} = (8\tau\tau_* \mathcal{A}/3)\epsilon_{skm} \overline{\mathsf{S}}_{mp}$. Adding all the terms one gets the expression given in Eq. (8) of the main text,

$$
\phi_{ijk} = C_{\mathrm{VC}}\, \epsilon_{ijl} \overline{\mathsf{S}}_{lk}; \quad \text{with} \quad C_{\mathrm{VC}} = 16\tau\tau_* \mathcal{A}/5. \quad \text{(A7)}
$$

One can estimate the dimensionless number C_{VC} as

$$
C_{\mathrm{VC}} = 16\tau\tau_* \mathcal{A}/5 \sim \tfrac{8}{5}(k_\mathrm{e} u\tau)(k_\mathrm{e} u\tau_*) \sim \mathrm{St}^2, \quad \text{(A8)}
$$

where we approximated $\mathcal{A} = \int E(k)k^2 \mathrm{d}^3 k \sim \tfrac{1}{2}u^2 k_\mathrm{e}^2$, taken $\tau \sim \tau_*$ and defined a Strouhal number $\mathrm{St} = k_\mathrm{e} u\tau$. For a flow dominated by a single scale $k_\mathrm{e} \sim k_\mathrm{f}$, the forcing scale. For a multi scale flow, like for Kolmogorov turbulence one should also keep the k dependence of $\tau(k) \propto k^{-2/3}$ say, and k_e could be larger by a logarithmic factor $\ln(k_\mathrm{d}/k_\mathrm{f})$ where k_d is the dissipative scale. However in a recent re-formulation of the dynamical quenching equation using local magnetic helicity density conservation (Subramanian & Brandenburg 2005, in preparation) we have recovered the Vishniac-Cho flux as a magnetic helicity flux, and in this case $k_\mathrm{e} \sim k_\mathrm{f}$. So it is reasonable to have $\mathrm{St} \sim uk_\mathrm{f}\tau < 1$, and hence $C_{\mathrm{VC}} < 8/5$.